NUMERICAL ANALYSIS OF MIXED-MODE FRACTURE PROCESSES

Pere C. Prat, Ignacio Carol and Ravindra Gettu

E.T.S. Enginyers de Camins, Canals i Ports
Universitat Politècnica de Catalunya
Gran Capità, s/n — 08034 Barcelona

Resúmen. En el presente trabajo se presenta un modelo de fisuración distribuída, que puede ser utilizado para análisis por el método de los elementos finitos de estructuras de hormigón, macizos rocosos y otros procesos de fractura en la corteza terrestre. El modelo, fundamentado en la técnica de los microplanos, puede representar la iniciación y la propagación de las fisuras bajo condiciones de tracción y corte. Las leyes de comportamiento se definen para un plano arbitrario, mientras que las ecuaciones constitutivas a nivel macroscópico se obtienen por combinación del efecto de todos los planos posibles. La coacción entre el comportamiento microscópico, a nivel de plano, y el macroscópico es del tipo estático. En este trabajo se presenta también un modo de fractura por corte que no presenta ambigüedades (Modo IIa), el cual está desacoplado del Modo I.

Abstract. A smeared crack model is described, which can be used in the finite element analysis of concrete structures, rock masses and crustal fault zones. The microplane-based approach can represent the initiation and propagation of tension and shear fracture. Behavioral laws for an arbitrary plane are prescribed and the macroscopic constitutive relations are obtained by combining the effects of all possible planes. A static constraint is imposed between the micro- and macro-relations. Also, an unambiguous shear mode (Mode IIa), which is uncoupled from the opening mode, is defined.

1. INTRODUCTION

The structural geometry, the presence of reinforcement and complex loading patterns prevent cracks in concrete structures from being planar or self-similar. Such behavior, known usually as mixed-mode fracture, has been observed in several types of brittle failure. One case, where the application of fracture mechanics is straightforward, is the cracking of dams [1]. The failure of reinforced concrete beams in diagonal tension [2] and torsion [3], have also been analyzed by nonlinear fracture mechanics. Other examples of mixed-mode fracture on concrete include the punching of slabs and plates, pullout of rebars and anchor bolts, and the failure of monolithic joints.

Another type of mixed-mode fracture is evident in the cracking of quasi-brittle materials such as concrete, rock and ceramics. Due to the heterogenous nature of these materials, the crack faces are uneven and rough, even when the cracks are macroscopically self-similar. The tortuosity is of the order of the size of the heterogeneities. Therefore, a crack propagating under shear loading not only undergoes slip but also opening. This phenomenon is critical in several aspects of concrete behavior such as shear transfer, aggregate interlock and the effects of confinement (see review in [4]).

It has been observed that shear failure of rock and, on a larger scale, fracture along fault zones involve bands of discontinuous tensile cracks (see discussions in [5] and [6]). Failure occurs when the tensile microcracks coalesce into a throughgoing macrocrack or fault. To account for these features, cohesive zone and crack band models based on fracture mechanics have been applied [7]. These are, to a certain extent, similar to those used for modeling concrete (see [8]). However, in geomechanics the effects of crack dilatancy and compressive stresses are of greater significance than in concrete [9].

In order to analyze the response satisfactorily, fracture parameters of the material need to be defined unambiguously and determined easily from experiments. The

identification of mixed-mode properties of concrete and rock, and in particular the shear fracture properties, is not straightforward. It has been shown that the mixed-mode fracture toughness increases significantly with a decrease in the Mode I component [10]. The shear fracture toughness also depends strongly on the crack dilatancy [11,12]. The inevitable coupling between the shear and opening modes could result in shear and mixed-mode fracture parameters that are influenced by the geometry of the test specimen and the magnitude of the compressive stresses across the crack. This also explains the wide discrepancy between the values obtained for the fracture toughness in Modes II and III [13]. On the basis of the crack model described here, an unambiguous shear mode of fracture, called Mode IIa, has been defined [14]. This can be described as uncoupled Mode II fracture devoid of the effects of dilatancy and transverse compression.

For analyzing mixed-mode fracture problems in concrete and geomaterials, finite element analysis seems to be the best available technique when coupled with the smeared crack approach. The effects of the crack tortuosity, the fracture process zone and the discontinuous cracking in fault zones are represented by a continuum with an equivalent constitutive relation. This method, however, has some drawbacks that have been discussed elsewhere [8,15-17]. In general, the constitutive model used should be formulated (1) to represent not only Mode I cracking but all the fracture modes, (2) with parameters defined in terms of material fracture properties, (3) such that cracks in different directions can occur simultaneously and co-exist, (4) to be used in conjunction with any model which represents the uncracked material, and (5) taking into account possible interactions between the fracture modes. The present model (proposed previously in [14] possesses these qualities, and in addition can handle crack initiation in shear, as well as tension. The microplane concept [18,19] is used to formulate the equivalent crack model. Laws for the behavior of a plane of generic orientation in the material are prescribed. The constitutive relations are obtained by mathematically combining the effects of all possible planes around a point.

2. CRACKING MODEL

2.1 Model for a single crack

The laws for a single crack are defined in terms of the normal (σ) and shear (τ) stresses applied on the crack plane. The two corresponding strain components are ϵ^{cr} and γ^{cr}. The crack is assumed to start when the stresses on the σ–τ space reach the hyperbolic "cracking surface" $F(\sigma,\tau)$=0 shown in Fig. 1a, (tensile stresses are positive). The "cracking function" F is defined by the following equation:

$$F = \tau^2 - (c - \sigma\tan\phi)^2 + (c - \chi\tan\phi)^2 \qquad (1)$$

where $\tan\phi$, c and χ are model parameters. From Fig. 1a one can distinguish two limiting situations: (a) cracking under pure tension with zero shear stresses (Mode I), and (b) cracking under shear and very high compression. In the latter case, the hyperbola approaches its asymptote, which in fact represents the Mohr–Coulomb criterion. We call this the "asymptotic Mode II" or Mode IIa of cracking. The hyperbola used provides a smooth transition for crack formation (mixed-mode cracking) between these two limiting states.

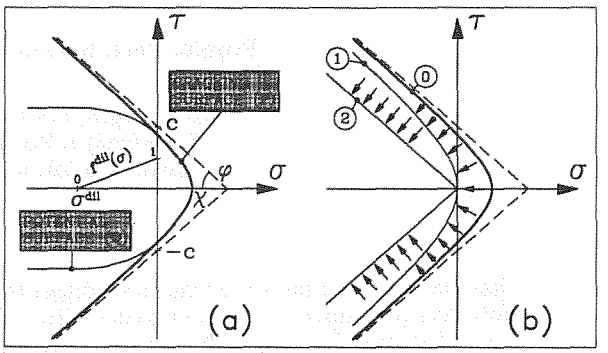

Fig. 1. (a) Hyperbolic cracking surface; (b) Evolution of the cracking surface.

As cracking progresses, the cracking surface shrinks so that the current stress point always remains on the surface. The initial shape of the cracking surface is represented by the curve labeled "0" in Fig. 1b, while its final shape depends on the mode of cracking. In pure tension (Mode I), the crack usually follows the weak interfaces between aggregate and hardened cement paste (Fig. 2a). The only kinematic condition once the crack is completely formed, is that both sides of the crack can separate from each other. Due to crack face roughness, the final surface is another hyperbola (curve "1" in Fig. 1b). On the other hand, Mode IIa would occur when shear displacement is kinematically admissible and no dilatancy is allowed. According to these restrictions, the only possible path for the crack is a straight line cutting through aggregates (Fig. 2b), and the corresponding surface is defined by a pair of straight lines representing pure frictional behavior (curve "2" in Fig. 1b).

We consider the evolution of the cracking suface for both modes as a single process, in which the evolution of parameters c and χ ($\tan\phi$ is assumed to remain constant) is controlled by a single internal variable w^{cr} (i.e. the work spent on the formation of the crack) defined as:

$$\begin{aligned} dw^{cr} &= \sigma d\epsilon^{cr} + \tau d\gamma^{cr}, && \text{if } \sigma > 0 \\ dw^{cr} &= (|\tau| - |\sigma|\tan\phi)|d\gamma^{cr}|, && \text{if } \sigma < 0 \end{aligned} \qquad (2)$$

Note that in compression the frictional work is not included in w^{cr} as already suggested elsewhere [20,21]. The parameters c and χ are assumed to decrease with w^{cr} from their initial values (c_0 and χ_0=f_t') to zero at $w^{cr} = g_f^I$ and $w^{cr} = g_f^{IIa}$, respectively (see Fig. 3). Here, f_t'=material tensile strength, g_f^I and g_f^{IIa}=fracture energies in Modes I and IIa. The variation is assumed to be linear in terms of the intermediate scaling function $\mathcal{S}$:

$$\mathcal{S}(\xi) = \frac{e^{-\alpha}\xi}{1 + (e^{-\alpha} - 1)\xi} \qquad (3)$$

where $\xi = w^{cr}/g_f^I$ and $\alpha = \alpha_\chi$ for parameter χ, and $\xi =$

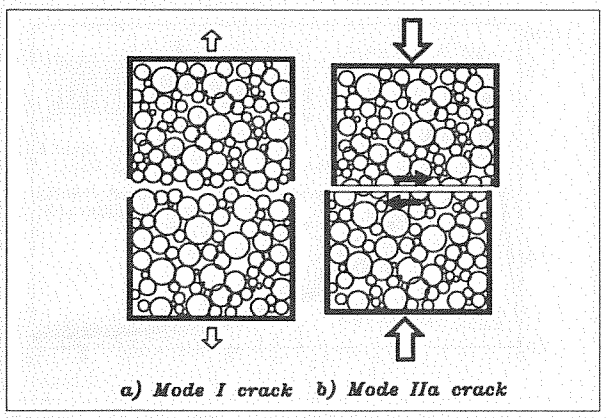

Fig. 2. Crack paths in the microstructure.

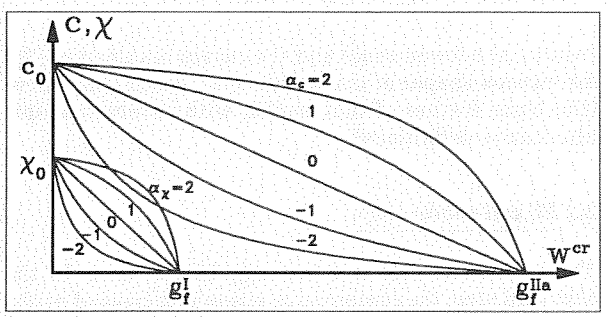

Fig. 3. Evolution of the cracking surface parameters with w^{cr}.

w^{cr}/g_f^{IIa} and $\alpha = \alpha_c$ for parameter c. This definition provides a family of descending curves for c and χ depending on the values of parameters α_χ and α_c (Fig. 4). A linear function is obtained if $\alpha = 0$, i.e. $\mathcal{S}(\xi) = \xi$.

To calculate the direction of the crack strain increments, we assume that they follow a path perpendicular to the "potential surface" Q=0 shown in Fig. 1a. In tension, this surface coincides with the cracking surface, i.e. the crack strains follow an associated rule. In compression, the rule is non–associated so that for high compression ($|\sigma| > |\sigma^{\text{dil}}|$) the crack shows no dilatancy. To this end, the horizontal component of the vector normal to the cracking surface is reduced by the factor f^{dil}, which is defined by a decreasing function of the compressive stress also represented in Fig. 1a. The equations defining Q are:

$$\frac{\partial Q}{\partial \sigma} = 2\tan\phi(c - \sigma\tan\phi)f^{\text{dil}}, \qquad \frac{\partial Q}{\partial \tau} = 2\tau \tag{4}$$

2.2 Formulation of the macroscopic model

To formulate a consistent macroscopic model including both continuum and cracks, a static constraint between macroscopic and crack plane levels has been assumed (i.e. the stresses acting on a crack plane, the microplane, are assumed to be equal to the resolved components of the macroscopic stress tensor). According to the static constraint, the stresses $\underline{s}_i = [\sigma, \tau]^t$ on a given plane of orientation $\underline{n}$, can be expressed in terms of the macroscopic stress tensor $\underline{\sigma}$ as:

$$\underline{s}_i = \underline{N}_i^t \underline{\sigma}, \qquad \underline{N}_i = \begin{bmatrix} \cos^2\theta & -\cos\theta\sin\theta \\ \sin^2\theta & \cos\theta\sin\theta \\ 2\cos\theta\sin\theta & \cos^2\theta - \sin^2\theta \end{bmatrix} \tag{5}$$

where θ is the angle between the normal to the crack plane i and the x–axis. The total macroscopic strain tensor is obtained from the contributions of the continuum and crack components:

$$\underline{\varepsilon} = \underline{\varepsilon}^{co} + \sum_{i=1}^{N_c} \underline{\varepsilon}_i^{cr}, \qquad \underline{\varepsilon}_i^{cr} = \underline{N}_i \underline{e}_i^{cr} \tag{6}$$

where N_c is the total number of active cracks and $\underline{e}_i^{cr} = [\epsilon^{cr}, \gamma^{cr}]^t$ is the crack strain vector in local coordinates. This kind of approach has already been used for similar purposes by other authors [22-24]. In some of these works devoted to cracking, however, different hypotheses concerning the conditions for crack formation and evolution lead to different formulations which, although less expensive in computational terms, are restricted to crack formation only in pure Mode I.

The direction of the crack strain increment is given by the plastic potential:

$$\mathrm{d}\underline{e}_i^{cr} = \left[\frac{\partial Q}{\partial \underline{s}}\right]_i \mathrm{d}\lambda_i \tag{7}$$

where $\mathrm{d}\lambda_i$ is a scalar factor. Note that in the present derivation repetition of subindex i does not imply summation, unless otherwise indicated.

As in classical plasticity, macroscopic stress increment $\mathrm{d}\underline{\sigma}$ is related exclusively to the continuum part of the strain tensor increment $\mathrm{d}\underline{\varepsilon}^{co}$:

$$\mathrm{d}\underline{\sigma} = \underline{D}^{co}\mathrm{d}\underline{\varepsilon}^{co} \tag{7}$$

From this point, a classical derivation leads to the final incremental relationship between macroscopic stress and strain tensor increments:

$$\mathrm{d}\underline{\sigma} = \underline{D}^{crco}\mathrm{d}\underline{\varepsilon}; \quad \underline{D}^{crco} = \underline{D}^{co}\left(\underline{I} - \sum_{i=1}^{N_c} \underline{N}_i \left[\frac{\partial Q}{\partial \underline{s}}\right]_i \left[\frac{\partial \lambda_i}{\partial \underline{\varepsilon}}\right]^t\right) \tag{8}$$

where $\underline{D}^{crco}$ is the tangent stiffness matrix of the equivalent medium representing continuum-plus-cracks. The vectors $\partial\lambda_i/\partial\underline{\varepsilon}$ are from the solution of an algebraic system of equations, which is obtained by enforcing the consistency condition for the cracking function F of every active crack.

2.3 Numerical implementation

The proposed cracking model has been implemented with linear elasticity for the uncracked continuum. It has a total of 10 parameters: 2 (E and ν) for the continuum model, and 8 ($\tan\phi$, c_0, χ_0, g_f^I, g_f^{IIa}, σ^{dil}, α_χ and α_c) for the crack model. A classical incremental plasticity procedure is used to integrate Eqs. 8. However, these equations are valid for a known set of active cracks but they do not specify the active cracks, and if some of them stop being active or start opening during a prescribed step. Establishing a correct scheme to check crack opening and closing is also an important part of the model implementation. As in previous microplane formulations, a fixed number of planes of pre-established orientation have been considered. 12 sample directions have been used in this work, distributed at constant intervals over a upper half hemicircle, and therefore, the same number of 12 internal variables (w^{cr} for each direction) need to be stored and updated during computations.

3. EXAMPLES OF APPLICATION

Two application examples are presented to demonstrate the performance of the proposed model for Mode I and mixed-mode (I+II) tests. Both are constitutive model examples, i.e. relations between stress and strain at a single material point carried out under 2–D plane strain conditions. The influence of the parameters g_f^I and g_f^{IIa} in the results has been investigated. The remaining parameters have been chosen as: E=1,000,000 psi, ν=0.18, $\tan\phi$=0.8785, c_0=416 psi, f_t'=230 psi and σ^{dil}=1000 psi. Also, a simple example of finite element analysis of Mode I fracture using the proposed model is presented. Similar analyses for mixed-mode fracture are currently under way.

3.1 Mode I tests

Two types of results are presented: results at the constitutive equation level and results for the boundary value problem (finite element analysis) level. The same set of constitutive subroutines are used for both types of analysis, whether they are called from a "single point" main program or from a finite element program, according to the scheme reported in [19].

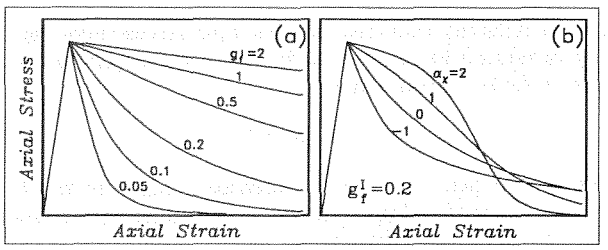

Fig. 4. Mode I cracking with different values of parameters: (a) g_f^I and (b) α_χ.

Fig. 4a shows the influence of parameter g_f^I on the stress–strain relation obtained for a pure tensile loading test. In the way the model has been defined, the area under each curve of the diagram is equal to the corresponding value of the parameter g_f^I. Fig. 4b shows the influence of parameter α_χ on the same relation. As expected, the shape of the softening law for χ (Fig. 3) is somehow reproduced in the σ–ϵ diagram: negative values of α_χ give σ–ϵ curves with a sharp drop at the beginning and a long asymptote reaching the x–axis slowly, while positive values give slowly decreasing curves at the beginning, then a sharp drop to zero (step–shaped variation). All curves have been obtained with constant values for the other parameters, thus retaining the same area under the load-deflection curve (value of g_f^I).

In Fig. 5, the results of the finite element analysis of a plain concrete beam tested under three-point bend conditions [25], and analyzed by Rots [26] are presented. For the sake of comparison, the number and order of the finite elements are the same used in [26], including the special integration rule with a single integration point in the horizontal direction for the elements ahead of the notch, along which the crack is to propagate. In Fig. 5, the results of the analysis, (load–displacement at the top midpoint of the beam) for three different values of parameter α_χ are shown, together with experimental

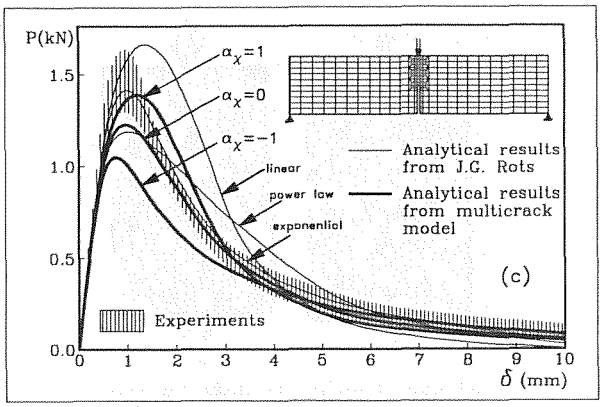

Fig. 5. Force–displacement diagram for the three-point bend tests and finite element mesh of Kormeling's beam.

results (shadowed zone) and the curves obtained in [26] for various shapes of the tensile σ–ϵ^{cr} descending curve (the basic feature of that model, with several possible alternative definitions).

3.2 Mixed-mode tests

The second example is a two–step biaxial test. In the first load step, the compressive stress is increased at the same time for both axes. Then, the strain is increased for the x–axis while the stress is kept constant on the y–axis. Various runs have been carried out with different values of σ_y and the fracture energies g_f^I and g_f^{IIa}. In this example the values of α_χ and α_c have been taken equal to zero. The results obtained are presented in Figs. 6–9. The cracks develop in two sample directions simultaneously, corresponding to planes symmetrically placed at 30° both sides of the x–axis. The final stress must have a residual value which can be statically determined in terms of σ_y, $\tan\phi$ and the angle of the crack, θ:

$$\sigma_x^\infty = \sigma_y \frac{\cos\theta \sin\theta - \sin^2\theta \tan\phi}{\cos\theta \sin\theta + \cos^2\theta \tan\phi} \qquad (11)$$

This feature is correctly reproduced after smoothly descending curves, with a change of slope at the point in which w^{cr} reaches g_f^I and χ vanishes (Figs. 6–8). The influence of g_f^I is less pronounced and almost nonexistent for a high lateral compressive stress (Figs. 6 and 9) as expected since that loading case represents almost a pure Mode IIa state.

4. SUMMARY AND CONCLUDING REMARKS

A new constitutive model for the analysis of concrete cracking in the context of a smeared finite element analysis has been presented. In this model, based on the microplane concept with static constraint, the laws for crack formation and evolution are established on a plane of generic orientation in terms of the stresses on that plane, which are assumed to be the resolved components of the macroscopic stress tensor. The behavior of the crack is governed by a hyperbolic cracking surface. This

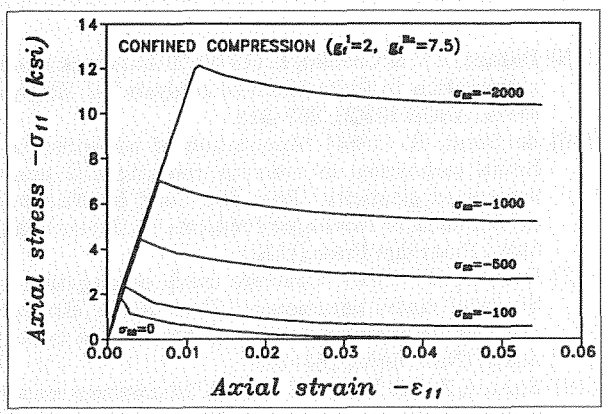

Fig. 6. Mixed mode cracking with different values of lateral stress.

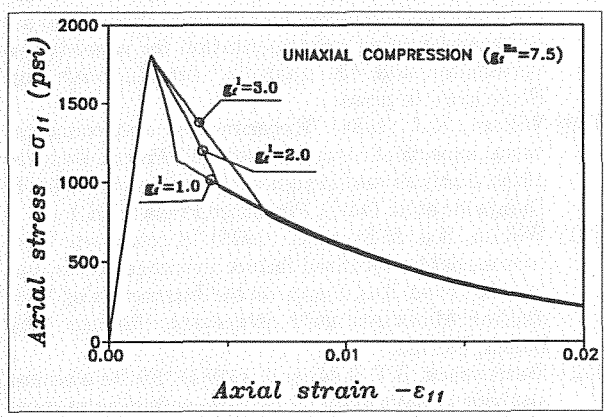

Fig. 7. Mixed-mode cracking in a uniaxial test with different values of g_f^I.

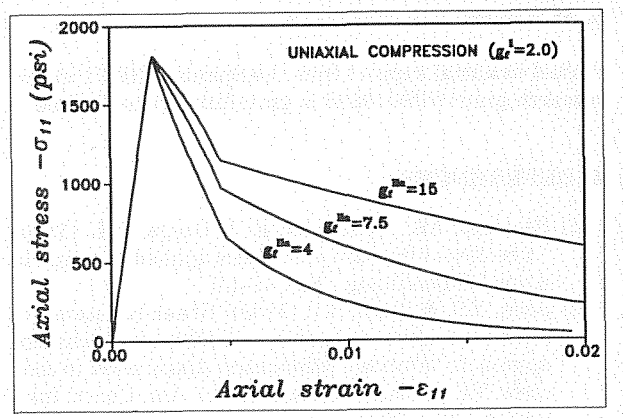

Fig. 8. Mixed-mode cracking in a uniaxial test with different values of g_f^{IIa}.

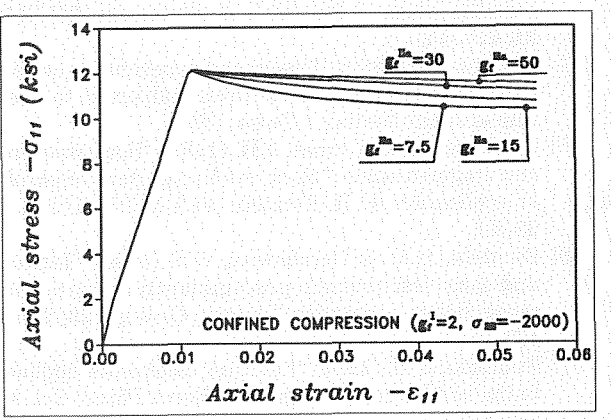

Fig. 9. Mixed-mode cracking under high confinement with different values of g_f^{IIa}.

surface shows two limiting situations for cracking: the classical Mode I in pure tension, and a newly introduced asymptotic Mode IIa for very high shear–compressive stresses with an independent g_f^{IIa} fracture energy in which friction is not included. Between these two limit states, the hyperbola provides a smooth transition so that a crack can start and develop under tension, shear–tension or shear–compression stress states. Both Mode I and Mode IIa fracture energies are parameters of the model. This makes the model adequate for smeared crack analysis in which automatic adjustment of parameters is performed at each integration point.

Although not yet supported by experimental evidence, the Mode IIa fracture provides new possibilities for theoretical interpretation and model development. The proposed definition of Mode IIa is an alternative to other definitions of a second mode of fracture (and its associated energy parameter) that can be found in the existing literature [23,24,27]. Compared to the latter possibilities, the proposed approach has some important advantages: it has a simple and clear definition in terms of the stresses on the crack plane, it is a "true" shear mode (the crack can start under shear–tension or shear–compression stress states, and not necesarily under pure tension), and it is defined completely uncoupled from the tensile Mode I, with independent energy parameters. In this context, the existing shear fracture tests under low or null confinement stresses [28,29] would represent combinations of Mode I and Mode IIa. New series of shear tests with increasing confining stress normal to the expected crack plane seem essential to clarify the adequacy of the model proposed.

The formulation of an overall macroscopic model including cracks in various directions and the possibility of using any existing continuum model for the uncracked material has also been presented. Its structure is of a multisurface non-associated plasticity type, from which the formulation of the tangent stiffness matrix and the step-by-step integration techniques have been borrowed. A number of pre-established sample directions over a circle around a point are checked systematically, and crack opening and arrest can be detected. The model has been implemented in a computer subroutine which performs strain-to-stress calculations and can be used in conjunction with either a "single-point" program or a finite element code.

Numerical results for both constitutive and finite element analysis show good qualitative agreement with experimental results as well as with other numerical results available in the literature. Numerical and experimental developments are currently under way in order to verify the hypothesis of Mode IIa fracture, and to extend the application of the model to the finite element analysis of mixed-mode fracture problems.

5. ACKNOWLEDGEMENTS

Partial financial support from the Spanish CICYT under research grant PB90–0598 is gratefully acknowledged.

6. REFERENCES

[1] Saouma, V.E., Brühwiler, E. & Boggs, H.L. (1990) "A review of fracture mechanics applied to concrete dams." *Dam Engng.*, **1**(1), 41–57.

[2] Jenq, Y.S. & Shah, S.P. (1989) "Shear resistance of reinforced concrete beams — a fracture mechanics approach." *Fracture Mechanics: Application to concrete.* V.C. Li & Z.P. Bažant (eds.), Am. Concr. Inst. (U.S.A.), 237–258.

[3] Bažant, Z.P., Şener, S. & Prat, P.C. (1988) "Size effect tests of torsional failure of plain and reinforced concrete beams." *Materials & Structures* RILEM, **21**, 425–430.

[4] Frénay, J.W. (1990) "Theory and experiments on the behaviour of cracks in concrete subjected to sustained shear loading." *Heron*, **35**(1).

[5] Fairhurst, C. & Cornet, F.H. (1981) "Rock fracture and fragmentation." *Rock mechanics from research to application.* H.H. Einstein (ed.), M.I.T. (U.S.A.), 23–48.

[6] Einstein, H.H. & Dershowitz, W.S. (1990) "Tensile and shear fracturing in predominantly compressive stress fields — a review." *Engrg. Geology*, **29**, 149–172.

[7] Rudnicki, J.W. (1980) "Fracture mechanics applied to the earth's crust." *Ann. Rev. Earth Planet Sci.* **8**, 489–525.

[8] Bažant, Z.P. & Oh., B.H. (1983) "Crack band theory for fracture of concrete." *Materials & Structures* RILEM, **16**, 155–177.

[9] Meredith, P.G., Ayling, M.R., Murrell, S.A.F. & Sammonds, P.R. (1991) "Cracking, damage and fracture in stressed rock: a holistic approach." *Toughening mechanisms in quasi-brittle materials.* S.P. Shah (ed.), Kluwer Academic (The Netherlands), 67–89.

[10] Swartz, S.E., Lu, L.W. & Tang, L.D. (1988) "Mixed-mode fracture toughness testing of concrete beams in three-point bending." *Materials & Structures* RILEM, **21**, 33–40.

[11] Izumi, M., Mihashi, H. & Nomura, N. (1986) "Fracture toughness of concrete for mode II." *Fracture toughness and fracture energy of concrete.* F.H. Wittmann (ed.), Elsevier Sc. (The Netherlands), 347–354.

[12] Luong, M.P. (1991) "Measuring toughness indices on brittle materials." *Fracture processes in concrete, rock and ceramics.* J.G.M. van Mier et al. (eds.), E.&F.N. Spon (U.K.), 727–736.

[13] Bažant, Z.P., Prat, P.C., & Tabbara, M.R. (1990) "Antiplane shear fracture tests (Mode III)." *ACI Materials Journal* **87**(1), 12–19.

[14] Carol, I. & Prat, P.C. (1990) "A statically constrained microplane model for the smeared analysis of concrete cracking." *Proc. 2nd. Int. Conf. on Computer Aided Analysis and Design of Concrete Structures, "Sci–C 1990."* N. Bićanić & H. Mang (eds.), Pineridge Press (U.K.), Vol. 2, 919–930.

[15] Bažant, Z.P. & Cedolin, L. (1979) "Blunt crack band propagation in finite element analysis." *J. Engrg. Mech.* ASCE **105**(2), 287–315.

[16] de Borst, R. (1984) "Application of advanced solution techniques to concrete cracking and non–associated plasticity." *Proc. Int. Conf. on Numerical Methods for Nonlinear Problems.* C. Taylor et al. (eds.) Pineridge Press (U.K.)

[17] Darwin, D. (1985) "Concrete crack propagation—Study of model parameters." *Proc. Finite element analysis of reinforced concrete.* C. Meyer et al. (eds.), ASCE (New York), 184–203.

[18] Bažant, Z.P. & Prat, P.C. (1988) "Microplane model for brittle–plastic material. I: Theory & II: Verification." *J. Engrg. Mech.* ASCE, **114**(10), 1672–1702.

[19] Carol, I., Bažant, Z.P. & Prat, P.C. (1992) "New explicit microplane model for concrete: theoretical aspects and unified implementation for constitutive verification and F.E. analysis." *Int. J. Solids and Structures,* in press.

[20] Willam, K.J. (1984) "Experimental and computational aspects of concrete fracture." *Proc. Computer aided analysis and design of concrete structures.* F. Damjanić et al. (eds.), Pineridge Press (U.K.)

[21] Willam, K.J. & Sture, S. (1985) "A composite fracture model for localized failure in cementitious materials." *Proc. 2nd. Symp. on the Interaction of Nonnuclear Munitions with Structures*, Panama City Beach, Florida.

[22] Pietruszack, S.T. & Mróz, Z. (1981) "Finite element analysis of deformation of strain–softening materials." *Int. J. of Numerical Methods in Engineering.* **17**, 327–334.

[23] de Borst, R. & Nauta, P. (1984) "Smeared crack analysis of reinforced concrete beams and slabs failing in shear." *Proc. Computer aided analysis and design of concrete structures.* F. Damjanić et al. (eds.) Pineridge Press (U.K.)

[24] Rots, J.G. & de Borst, R. (1987) "Analysis of mixed–mode fracture in concrete." *J. Engrg. Mech.* ASCE, **113**(11), 1739–1758.

[25] Kormeling, H.A. & Reinhardt, H.W. (1983) *Determination of the fracture energy of normal concrete and epoxy modified concrete.* Report 5-83-18, Stevin Lab., Technische Universiteit Delft (The Netherlands).

[26] Rots, J.G. (1988) *Computational Modeling of Concrete Fracture.* Ph.D. Thesis presented to the Technische Universiteit Delft, The Netherlands.

[27] Oliver, J., Cervera, M., Oller, S. & Lubliner, J. (1990) "Isotropic damage model and smeared analysis of concrete." *Proc. 2nd. Int. Conf. on Computer aided analysis and design of concrete structures "Sci–C 1990."* N. Bićanić & H. Mang (eds.), Pineridge Press (U.K.), Vol. 2, 945–958.

[28] Arrea, M. & Ingraffea, A.R. (1981) *"Mixed–mode crack propagation in mortar and concrete."* Rep. 81–13. Dept. of Struct. Engrg., Cornell Univ., Ithaca, New York.

[29] Bažant, Z.P. & Pfeiffer, P.A. (1986) "Shear fracture tests of concrete." *Materials & Structures* RILEM, **19**, 111–121.